Simulation of Flow in the Human Upper Airways Modeled as a Piping System Using the Hydraulic Diameter

Thor Gudmund Weisz [a,*], Bernhard Müller [b], Reidar Kristoffersen [c],

[a,b,c] *Department of Energy and Process Engineering, NTNU, Trondheim, Norway*
[*] *thor.weisz@gmail.com*

Abstract

Obstructive sleep apnea (OSA) is a medical condition characterized by repetitive obstructions in the human upper airways during sleep. Recent estimates from the United States show that the condition impacts 15% to 20% of the adult population. OSA treatment can be subdivided into surgical and non-surgical approaches. Non-surgical approaches such as continuous positive airway pressure (CPAP) devices have the highest success rates when used correctly. However, these approaches have low patient compliance due to the invasive nature of the devices during sleep, leaving surgery as a viable alternative for many. Predicting the outcome of OSA surgery is difficult due to the complex nature of both the airways and the surgeries themselves. CFD modeling of the airways is a helpful way to gain valuable insights into the flow structures and the impact of individual surgeries on the airways. However, CFD is not a viable approach for each patient-specific case due to its time-consuming nature. A pragmatic model has been created to predict the outcome of OSA surgery on a patient-specific basis to produce valid surgical estimates fast to be used by non-CFD engineers. The model transforms the human upper airways into a piping system by applying the hydraulic diameter equation on geometries created from CT scans. This paper aims to validate the use of the hydraulic diameter given by $D_h = 4 \cdot \frac{A}{P_e}$, where A is the cross-sectional area and P_e is the wetted perimeter, on the complex geometries of the nasal cavity and to provide a novel equation for the hydraulic diameter in the nasal cavity. The proposed hydraulic diameter equation is given by $D_h = C_{D_h} \cdot \frac{A}{P_e}$ where C_{D_h} is the hydraulic diameter coefficient. Airflow has been simulated through a simplified geometry using CFD to validate the hydraulic diameter and find an updated equation. Pragmatic model simulations using the hydraulic diameter have been compared to the results from CFD simulations to assess the pragmatic model's accuracy. The results showed that the original hydraulic diameter did not give entirely accurate results and that the novel equation using $C_{D_h} = 3.71$ gave the pragmatic model better accuracy for the validation cases. Tuning the parameter C_{D_h} for flow in an OSA patient's upper airways, the pragmatic model succeeded in quite accurately reproducing the area-averaged pressure in the patient's upper airways.

1. Introduction

Obstructive sleep apnea (OSA) is a sleep disorder characterized by repeated collapses of the upper airways during sleep. These collapses obstruct airflow, leading to loss of oxygen intake and a build-up of CO_2, which can cause daytime symptoms such as drowsiness or loss of functioning while seemingly getting enough sleep (Punjabi, 2008). It may cause a stroke or a heart attack in more severe cases. There are several surgical and non-surgical treatment options that help to alleviate or remove OSA entirely. The most common treatment is the non-surgical use of a sleeping mask which provides a constant pressurized flow through the airways, removing the possibility of airway collapse. Of these devices, the most common one is the continuous positive airway pressure device (CPAP) which is highly effective when properly used. However, patient compliance is a prominent issue with such devices (Sawyer et al., 2011). These factors leave surgical treatment as a viable option in many cases, although it is more invasive in the short term. Since OSA first was described in the middle of the 10^{th} century (Gharibeh and Mehra, 2010), there have been many medical advances in surgical treatment options for OSA. Although significant advances have been made in OSA treatment, the outcome of surgery is still not entirely predictable (Kezirian et al., 2004; Friedman et al., 2005). There have been marginal improvements in some cases, and in more severe cases, OSA has worsened after surgery.

1.1. Fluid Mechanics in OSA

Computational fluid dynamics (CFD) and widely available computed tomography (CT) image segmentation tools have made it possible to create patient-specific 3D models for airway analyses rapidly (Kim et al., 2013). Fig. 2 shows a 3D model of the human upper airways of an OSA patient prior to surgery. With appropriate verification and validation, CFD becomes a great and trustworthy tool that makes model testing much faster than its experimental counterpart. Even though computational capacity has seen exponential growth, detailed CFD simulations are still computationally expensive. Using CFD software to acquire accurate and trustworthy results requires an experienced engineer, making it a less viable choice for medical doctors to use in patient-specific cases. The pragmatic simulator developed through Weisz' specialization project (Weisz, 2021) and further improved through the same author's master's thesis (Weisz, 2022) is a proposed method for combining the accuracy of CFD

with low computational cost and user-friendliness.

1.2. Pragmatic Model

The pragmatic model is a proposed 1D flow simulator that takes in cross-sectional data from the upper airways of a patient with OSA and converts it into a piping system. Fig. 3 represents the upper airways of an OSA patient, while Fig. 4 is a visual representation of the upper airways as a piping system, used for the pragmatic simulations. The area-averaged gauge pressure is calculated using the Bernoulli equation with losses from cross-section to cross-section (Cengel and Cimbala, 2010). The geometrical variations in the geometry lead to additional pressure losses, which are modeled using known relations for pipes and included in the Bernoulli equation with losses. A doctor can perform the pragmatic calculations and the results can give insights into the current state of the patient's airways, and further help determine what type of surgery to perform.

1.3. Hydraulic Diameter

In the pragmatic model described, the unorthodox transformation of the human upper airway cross-sectional geometry to a pipe using the hydraulic diameter has been made. Fig. 1 shows a representation of this transformation for a cross-section in the nasal cavity which is further expanded to include the complete upper airways in Fig. 4. Since this is not a common approach, validation material is challenging to find. As the airway from the nasopharynx and down has a less complex shape and only one passage, the hydraulic diameter assumption is assumed to be accurate for this anatomical region. Although a validation using the entire geometry would be beneficial, it would yield patient-specific results and might not apply to all OSA patients. It would also be difficult to validate these results since experimental data for velocity and pressure in OSA patients' upper airways are unavailable. This led to the proposal of two simplified test cases used for simulations with the CFD tool Ansys Fluent (ANSYS, 2021*a*). The results led to a redefinition of the hydraulic diameter for this specific case after comparison with results from the pragmatic simulation.

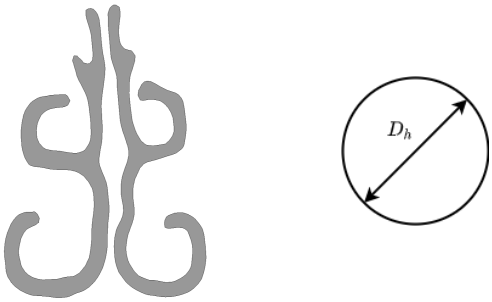

Figure 1: Representation of the conversion from a cross-section in the nasal cavity to a circle with the hydraulic diameter D_h.

2. Theoretical Background

In this paper, the flow simulations from the pragmatic model described in this section are validated using simulations with the commercial CFD software Ansys Fluent. The two simulators have different sets of governing equations solved through the simulations. Both sets of governing equations will be presented in this section of the paper.

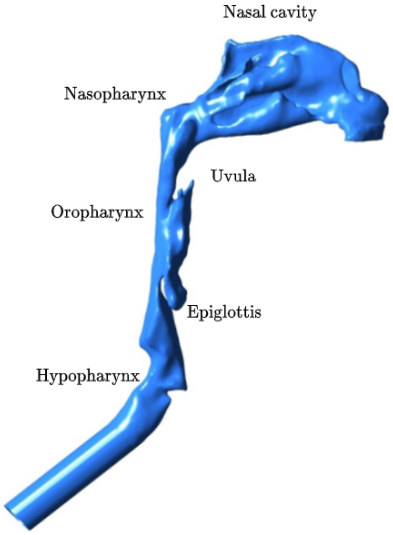

Figure 2: 3D model of the human upper airways adapted from Jordal's master's thesis (Jordal et al., 2017).

2.1. Governing Equations for the Pragmatic Model

The governing equation for the pragmatic model is the Bernoulli equation with losses used to calculate the pressure through the human upper airways. The Bernoulli equation with losses between arbitrary points 1 to 2 along a streamline is given as (Cengel and Cimbala, 2010):

$$\frac{p_1}{\rho g} + \alpha_1 \frac{V_1^2}{2g} + z_1 = \frac{p_2}{\rho g} + \alpha_2 \frac{V_2^2}{2g} + z_2 + h_L \qquad (1)$$

where p_1 and p_2 are the pressures and V_1 and V_2 are the velocities at point 1 and 2, respectively. z_1 and z_2 correspond to the height of each point, while α_1 and α_2 are the kinetic energy correction factors. ρ is the density of the fluid and g is the gravitational acceleration. h_L is the loss term which accounts for irreversible losses in the equation. Through solving (1) for the pressure at point 2 and substituting in an index notation, the pressure is given as

$$p_i = p_{i-1} + \rho \frac{\alpha_{i-1} V_{i-1}^2 - \alpha_i V_i^2}{2} + \rho g (z_{i-1} - z_i) - \rho g h_{L,i}, \qquad (2)$$

where $i-1$ and i refer to cross-sections along the same streamline. This pressure corresponds to the gauge pressure in the pragmatic model, as the reference pressure is assumed to be atmospheric.

2.2. Losses

The loss term in equation (1) is comprised of both minor and major losses, where major losses are frictional losses and minor losses are caused by losses from geometrical changes in a pipe (Cengel and Cimbala, 2010, p. 364). The minor losses in the pragmatic simulator are given by

$$h_{L,minor,i} = \sum_{j=1}^{m} K_{L,j} \frac{V_j^2}{2g}, \qquad (3)$$

where j is a geometric component causing a minor loss in section i of the airways and $K_{L,j}$ is its minor loss coefficient. The major loss is given by

$$h_{L,major,i} = f_i \frac{L_i}{D_{h,i}} \frac{V_i^2}{2g}, \qquad (4)$$

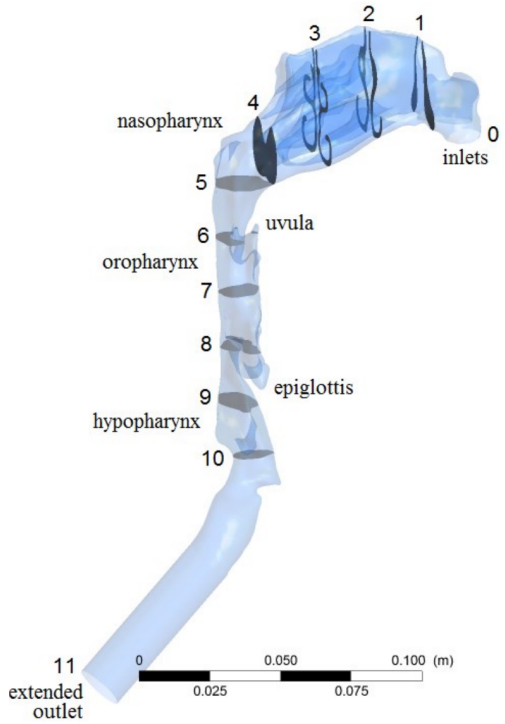

Figure 3: Locations of cutplanes used for the extraction of the area-averaged gauge pressure in the CFD investigation of the human upper airways (Aasgrav, 2017).

where i is the section of the pipe between cross-sections $i-1$ and i. L_i is the length of the section, and $D_{h,i}$ is its hydraulic diameter.

2.3. Diffuser Effect

The minor losses in Eq. (3) include losses that occur due to gradual expansions. Results from the pragmatic simulations show that additional loss modeling may be required in these regions. These additional losses due to flow separation are modeled through a pressure-recovery coefficient given as (White, 2008, p. 398)

$$C_p = \frac{p_e - p_t}{p_{0t} - p_t}, \tag{5}$$

where p_e and p_t are the pressure at the exit and throat of the diverging nozzle respectively and p_{0t} is the stagnation pressure at the throat. To include this as an additional loss it can be solved for p_e after obtaining a value for C_p and adding it to Eq. (2).

2.4. Hydraulic Diameter

The hydraulic diameter is given by the equation

$$D_h = 4 \cdot \frac{A}{P_e}, \tag{6}$$

where A is the cross-sectional area of the geometry and P_e is the wetted perimeter. In the investigation, a variation of the hydraulic diameter is proposed, which is given by

$$D_h = C_{D_h} \cdot \frac{A}{P_e}, \tag{7}$$

where C_{D_h} is the "hydraulic diameter coefficient" which replaces the constant 4 in the original equation.

2.5. Volumetric Flow Rate

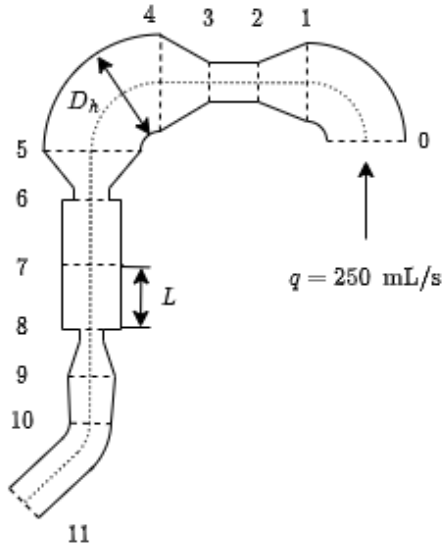

Figure 4: Piping representation of the human upper airways used for simulations using the pragmatic model. The numbered locations correspond to the cutplanes in Fig. 3.

The velocity is one of the input variables in Eq. (2) and therefore needs to be calculated. Since the flow rate is known, the velocity can be calculated using the incompressible volumetric flow rate

$$Q = V_i A_i = \text{constant}. \tag{8}$$

In this equation V_i is the velocity and A_i is the cross-sectional area of cross-section i.

2.6. Governing Equations for CFD

In the commercial CFD software Ansys Fluent (ANSYS, 2021*a*) the Navier Stokes equations are solved on a discretized mesh using the finite volume method. The continuity equation and the momentum equation, which make up the Navier-Stokes equations, are solved for each cell. Since the Mach number is much lower than 0.3, the incompressible variants of the equations have been used. The incompressible continuity equation is given by

$$\frac{\partial u_i}{\partial x_i} = 0, \tag{9}$$

where u_i is the velocity component in the $x_i -$ direction where $i = 1, 2, 3$. The incompressible momentum equation is given by

$$\frac{\partial u_i}{\partial t} + u_j \frac{\partial u_i}{\partial x_j} = f_i - \frac{1}{\rho}\frac{\partial p}{\partial x_i} + \nu \frac{\partial^2 u_i}{\partial x_j \partial x_j}. \tag{10}$$

f_i is the i^{th} component of the gravitational acceleration, where $i = 1, 2, 3$. ν is the kinematic viscosity, which is a constant for this case. Einstein summation is assumed for equations (9) and (10).

3. Methodology

As mentioned in the introduction, converting two ducts into one using the hydraulic diameter is not a common approach. To the knowledge of the authors, this conversion has not been used for flow calculation using the proposed method. Therefore, the procedure is explained in detail in the following section, along with justifications for the choices made.

3.1. Numerical Setup

A simple numerical case was chosen to validate the use of the hydraulic diameter on cross-sections from the human upper airways. For simplicity, a rectangular duct was chosen as the foundation of the simplified geometry. With a duct as the basis a wall was introduced to the geometry giving the duct a divided geometry, further mimicking the geometry in the nasal cavity. The separating wall is the simple geometry's counterpart to the septum, the cartilage which divides the nasal passage in the airways (Matthias, 2007). One of the ducts was created more narrow than the other because of the prevalence of deviated septums in OSA cases. A deviated septum is a deformation of the cartilage and bone wall separating the nasal passages, which impacts the many functions of the nasal cavity (Fettman et al., 2009). Therefore, the variation in geometry between the two passages in the numerical geometry was implemented to generalize the test case. Fig. 5 shows the setup and the dimensions of the different passages. The length of the wall was chosen to allow the flow to develop while not necessarily becoming fully developed, as the flow in the nasal cavity does not become fully developed due to the short entry length and its varying geometry. Two test cases were chosen since differences will occur in the various patient-specific upper airways. Both of the test cases have the same overall dimensions apart from the leading and trailing ends of the wall. One numerical case has a wedge at the leading and trailing ends of the wall, while the other has flat ends.

3.1.1. Wall with Wedged Ends

In the human upper airways, flow separation is likely to occur at various stages because of the complexity of the geometry. However, for the simple generalizable case presented in this paper, investigating a non-separated flow is of interest, possibly yielding a better base case for future comparison. To avoid flow separation leading into the region with two passages, a 10° wedge is placed in front of the wall. The walls on either side are flat, which effectively leads to an angle of 5° for either passage. For a circular diffuser, flow separation has been found to occur in the range $1000 \leq \mathrm{Re} \leq 4000$ (Sparrow et al., 2009) giving a comparable case downstream of the wall. The Reynolds number of the flow in both of the single duct sections, prior to and post the separated passages, was $\mathrm{Re} = 2500$. Although the test case is not circular, it was chosen as a case with a lower chance of separation than its wedge-less counterpart. The dimensions of the computational domain have been taken from the height and width of a nasal cavity cross-section at its largest point. The left figure in Fig. 1 shows the largest cross-section. The largest section of the airways was measured using the 3D geometry from a patient who showed great improvement in OSA post-surgery. The same geometry used (Aasgrav, 2017).

3.1.2. Wall with Flat Ends

An alternative numerical setup to the wedged setup presented in the section above was tested. This alternative setup was proposed to capture flow separation and recirculation which are likely to occur in the complex human upper airways (Martonen et al., 2002). The alternative setup chosen is identical to Fig. 5 apart from the leading and trailing ends of the separating wall, which in the alternative case are flat. The alternative setup is shown in Fig. 6. The flat leading and trailing ends of the separating wall are hypothesized to cause flow separation and recirculation, similar to the flow structures found in a backward-facing step (Lee and Mateescu, 1998). This is meant to aid in the validation of the hydraulic diameter by providing more test data more closely resembling actual human upper airway flow structures.

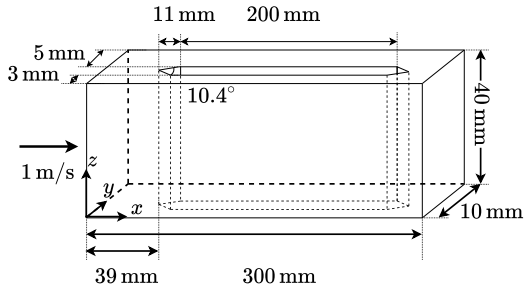

Figure 5: Numerical setup with 10° wedges at both ends of the separating wall.

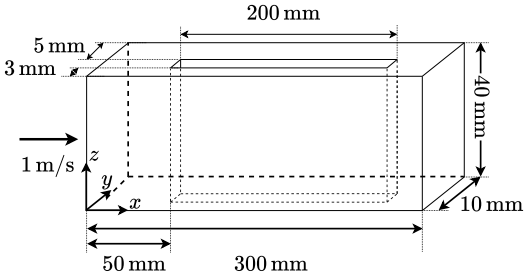

Figure 6: Numerical setup where the leading and trailing ends of the separating wall are flat.

3.2. Inlet and Outlet Boundary Conditions

For both test cases, the boundary conditions at the inlet and outlet, respectively, were the same. In both cases air with a kinematic viscosity of $\nu = 1.6 \cdot 10^{-5}$ was used as the fluid. A fully developed laminar flow was given as the inlet condition. The fully developed flow was found by extending the numerical domain prior to the inlet by an entry length of 800 mm, with a uniform flow of $V = 1$ m/s at the inlet of the extended domain. The entry length was found using the equation for a nondimensional hydrodynamic entry length for a laminar flow (Cengel and Cimbala, 2010, p. 342). The inlet velocity was found by calculating the Reynolds number using the actual human upper airway geometry and is based on a flow rate of 250 mL/s (Aasgrav, 2017). The outlet condition specified the gauge pressure and is set to 0 Pa at the end of the flow domain. The outer and internal separating walls were treated with no-slip boundary conditions.

3.3. Grid Generation

The mesh for both cases was created using Ansys Meshing (ANSYS, 2021*b*), a part of the Ansys simulation environment, where all of the simulations were carried out. With the help of the mesh creator and Ansys Workbench (ANSYS, 2021*c*), several different grid configurations were tested to find a grid that would provide a grid-independent solution. The result from the pragmatic model simulations was the area-averaged gauge pressure. This was a natural quantity to check when performing the mesh independence study. The grid was created by predetermining the number of subdivisions along the outer horizontal edges, the horizontal edges along the separating wall, and the outer vertical edges. To create the mesh,

the number of division along the outer edges and along the wall's edges in the x-direction was set to 300, thus giving the numerical domain 300 cells in the x-direction. 8 cells were used in the y-direction and 40 cells were used in the z-direction, both created by setting the number of divisions along the outer edges in their respective directions to 8 and 40 respectively. In Ansys Meshing (ANSYS, 2021*b*) the behaviour of these sections was set to "hard" to create a structured mesh mostly containing hexahedral cells. This meshing scheme made it possible to generate meshes at different scales with the same proportions in a controllable way. Different resolutions for the mesh were created and simulated while controlling the selected parameter, the gauge pressure. The meshes with a slightly coarser resolution gave similar pressure values for the control plane. Therefore, the mesh with a higher number of cells was chosen for further simulations since the control parameter remained reasonably constant. The mesh independence study was only performed on the numerical domain with a 10° wedge. The same grid generation technique and resolution were applied to the case with flat wall ends.

3.4. Tuning the Hydraulic Diameter

Altering the hydraulic diameter given by Eq. (6) is proposed to match the results from the CFD investigations more accurately. A novel method to tune this parameter was to define a hydraulic diameter coefficient, C_{D_h}. The hydraulic diameter coefficient replaces the constant, 4, in Eq. (6) to obtain a new equation given by (7) allowing the possibility to find a coefficient that better represents the present case. The method involved running the CFD simulations described in this paper along with the pragmatic simulations and comparing the results from both. The pragmatic simulations' input were the flow rate, cross-sectional area and the wetted perimeter from evenly spaced cross-sections along the numerical geometries. The pragmatic model was modified only to include the frictional losses introduced through the major loss term in Eq. (4)when validating the hydraulic diameter. The hydraulic diameter is present in both the Reynolds number and the loss term itself, leading to a negative squared inverse correlation between the pressure and the hydraulic diameter. This correlation implies that a decrease in the hydraulic diameter leads to a decrease in the pressure slope. Pragmatic simulations were run for hydraulic diameter coefficients in the range $3 \leq C_{D_h} \leq 4.2$ to compare the CFD simulations and the pragmatic simulations. The residual sum of squares (RSS)(Wikipedia contributors, 2022) was calculated for each pragmatic simulation. The equation for RSS is given by

$$RSS = \sum_{i=1}^{n} (y_i - f(x_i))^2, \tag{11}$$

where y_i is the i^{th} component of the value to be predicted (the area-averaged gauge pressure from CFD simulation) and $f(x_i)$ is the i^{th} component of the predicted value (the area-averaged gauge pressure from the pragmatic model). The RSS value was calculated using pragmatic and CFD gauge pressures from the middle of the wall to the end of the walled section, i.e. $150\,\text{mm} \leq x \leq 200\,\text{mm}$ in Fig. 5 and Fig. 6. This was done to reduce the impact of inaccuracies in the error estimation in the entrance regions of the split geometries. In these regions, deviations are expected due to the simple nature of the pragmatic simulations. The hydraulic diameter coefficients could then be obtained by minimizing the error in this region.

3.5. Minor Losses and Diffuser Effects

With the pragmatic model using loss relations known from piping systems, the accuracy of these relations is important. An effect seen in the results of the pragmatic simulations is a nonphysical pressure recovery where the human upper airway geometry has an expansion. The relations for expansions used in the pragmatic model did not accurately model the pressure difference seen in the CFD simulations (Weisz, 2022). Therefore, it was proposed that the effects of flow separation were more significant than initially thought. To further investigate this increased flow separation and model it accurately, the effects were included in the validation simulations presented in the present paper. This was implemented at the end of the walled section, where the nasal passages coincide. The Bernoulli equation with losses Eq. (1) takes flow separation into account though minor losses given by Eq. (3). However, the pressure recovery found through the pragmatic flow simulations was too large. This occurs when the two passages in the geometry coincide downstream of the separating wall and there is an increase in the cross-sectional area for both passages. This effect can be taken into account through added diffuser losses for these sections. These losses were calculated using Eq. (5) by using the CFD gauge pressure to calculate the pressure recovery coefficient C_p, using Eq. (5). The exit pressure, p_e, in Eq. (5) was the CFD gauge pressure from the cross-section downstream of the expansion, and the throat pressure, p_t, in Eq. (5) was the gauge pressure from the cross-section upstream of the same expansion. The calculated C_p values for the expanding sections were included in the pragmatic model by solving Eq. (5) for the exit pressure p_e using the area-averaged gauge pressure from the pragmatic model, p_{i-1}, as the throat pressure, p_t. This was used as p_i in the pragmatic model instead of using Eq. (2) to calculate p_i for this section, leading to a larger, more physically accurate pressure loss in the relevant region.

3.6. Verification of the Numerical Code

A crucial part of any CFD simulation is verifying the accuracy of the code used for simulations. In the present case, this step was done through a simplification of the numerical domain. The 3D domain was simplified to a 2D domain with the same height as the 3D domain, 40 mm, and long enough for the flow to become fully developed. The fully developed flow was found by using a domain which was 7000 mm in length, giving the flow the opportunity to become fully developed. The grid for the verification case was created using Ansys Meshing (ANSYS, 2021*b*), where a structured grid with rectangular cells was created. The mesh had 1000 cells in the flow direction, where a bias which decreased the cell size from the inlet to the outlet was included to achieve similar cell dimensions as in the 3D case towards the end of the domain. 40 cells were used in the y-direction with even spacings. The inlet velocity was chosen to be $V = 1\,\text{m/s}$ to achieve a Reynolds number of $\text{Re} = 2500$ using the height of the domain as the length scale and $\nu = 1.6{\cdot}10^{-5}$ as the kinematic viscosity. The simulations were carried out using Ansys Fluent (ANSYS, 2021*a*), using the same settings as the full 3D simulations. The results from the verification were compared to the analytical solution of a plane Poiseuille flow (Cengel and Cimbala, 2010, p. 468). Fig. 7 compares the two solutions and shows a high degree of accuracy in the numerical simulations compared to the analytical solution. Fig. 7 also shows the development of the flow, at the locations $x = 0.05$, 2 and 6.9 m, where x is

the downstream distance from the inlet located at $x = 0$ m. The flow profiles show an expected development with the flow reaching its fully developed state at $x = 6.9$ m. Since these results correspond to their analytical counterpart, the solver was considered an accurate enough standard for further numerical investigation.

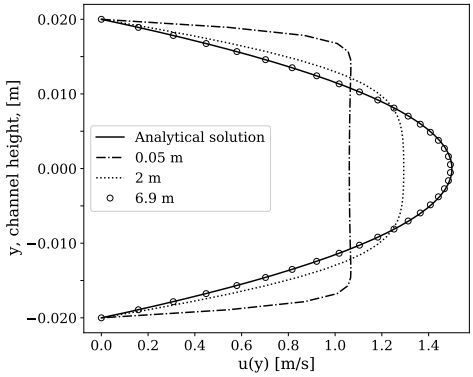

Figure 7: Fluid flow profiles at the locations $0.05, 2$ and 6.9 m downstream from the inlet. The flow profile reaches the analytical solution close to the end of the simulation domain, $x = 6.9$ m. The analytical solution is given for a fully developed plane Poiseuille flow.

3.7. Pragmatic Simulations

The pragmatic simulations were run using input data found using the numerical geometries. The area-averaged gauge pressure was extracted when the CFD simulations were completed. The pressure was extracted at evenly spaced cross-sections along the length of the numerical domain. The pragmatic model's input for each location is the cross-sectional area, the perimeter and the flow rate for the given simulation. The cross-sectional area and the perimeter of each cross-section were calculated based on the numerical geometries' dimensions shown in Fig. 5 and Fig. 6, the extracted values are shown in Tab. 1. The flow rate was calculated using the area-averaged input velocity $V = 1$ m/s. The flow rate could then be converted into the velocity at the various cross-sections in the wall-separated region using equation (8). The pragmatic simulations were then carried out and the area-averaged gauge pressure from both the pragmatic simulations and the CFD simulations could be compared.

Table 1: Cross-sectional area and perimeter calculated using dimensions from Fig. 5 and Fig. 6, where the dimensions at $x = 45$ mm only apply to the wedged case.

x [mm]	A [mm^2]	P_e [mm]
0	400	100
45	356.36	177.82
150	320	176

4. Results and Discussion

The results from the validation simulations are to be applied to the pragmatic model to accurately represent the flow through predicting the area-averaged gauge pressure. The area-averaged gauge pressure from the pragmatic simulations and the CFD simulations are compared to assess the accuracy of the standard hydraulic diameter Eq. (6) and find an accurate fit for the hydraulic diameter coefficient C_{D_h} in Eq. (7). Fig. 8 and 9 show the results from both simulations along with the initial pragmatic results using Eq. (6), which are the uppermost curves The initial results revealed deviations from the CFD simulations, most notably the slope of the area-averaged gauge pressure. The slope of the pragmatic curve was initially too flat and was altered through varying the hydraulic diameter coefficient C_{D_h}. In the Bernoulli equation with losses (1) the hydraulic diameter D_h is inversely correlated to the pressure through its representation in the loss term h_L, given by Eq. (4). However, as the term is negatively signed, the pressure gradient and the hydraulic diameter become correlated, leading to predictable changes when tuning the coefficient C_{D_h}. Changing the hydraulic diameter coefficient and introducing losses from the pressure-recovery coefficient gave more accurate results when compared to the CFD simulations. The effects on the pragmatic model from both of the numerical validation cases are presented and discussed in the following subsections.

4.1. Wall with Wedged Ends

Fig. 8 shows the results from both the CFD simulations and the pragmatic simulations in the case where the wedge is present. The results show an expected decline in the area-averaged gauge pressure through the geometry. The pragmatic simulations have a linearly decreasing pressure in the middle section, where the separating wall is located, but with varying slopes. The CFD simulation has a less linear shape in the section with the separating wall. However, it has a linear trend further downstream. Compared to the CFD simulations, it has a slight additional pressure loss as the duct is split up, and a slight pressure gain at the opposite side. The initial pragmatic results have similar trends but with inflated loss values as well as pressure gain. Using the error minimization approach described in the methodology section, $C_{D_h} = 3.73$ was found as the optimal hydraulic diameter coefficient. A visualization of the optimization is shown in Fig. 10. The pressure-recovery coefficient was calculated by applying pressure values from the CFD simulations to Eq. (5). This showed an improvement in accuracy downstream of the walled section.

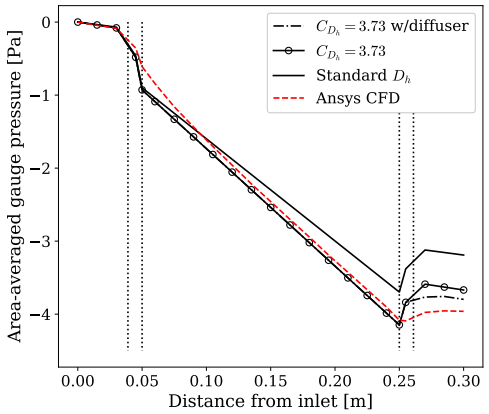

Figure 8: Results from Ansys Fluent and corresponding pragmatic simulations for simulations with a 10° wedge at both ends of the separating wall. The vertical dotted lines indicate the wedge locations.

4.2. Wall with Flat Ends

The alternative flow situation used to study the hydraulic diameter is also investigated. For this case, the separating

wall has flat ends instead of wedges. The aim of this was to study the effects of tuning the hydraulic diameter coefficient, C_{D_h}, and comparing it to the wedged case to find out how the hydraulic diameter coefficient would deviate from the initial results. This was to study the reliability and generalizability of the results obtained in the wedged case. The results from these simulations are displayed in Fig. 9. Minimizing the RSS value for these simulations gave $C_{D_h} = 3.69$ as the hydraulic diameter coefficient with the highest accuracy. Similarly to the case with 10° wedges, applying the increased pressure recovery coefficient to the pragmatic simulations gave a result closer to the CFD simulations. Due to the nature of the geometry with its sudden geometrical changes, the pragmatic model has sudden pressure changes at the beginning of the walled section and at the end, with a pressure loss and a pressure gain respectively. The same procedure for finding the pressure recovery coefficient was used. In the case with flat ends, this gave a highly accurate result. This implies that there is more flow separation in the non-wedged case. However, this increased accuracy may be due to the sudden changes, which make the pressure recovery coefficient from the CFD simulations easier to find. The increased accuracy using the pressure recovery coefficient in the wedge versus the non-wedged case is thus inconclusive. However, the use of a pressure recovery coefficient in general is promising.

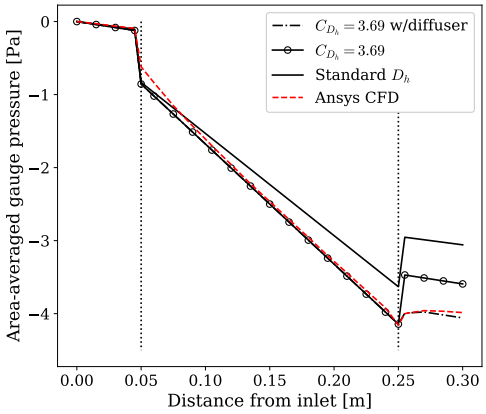

Figure 9: Results from Ansys Fluent and corresponding pragmatic simulations for the simulations with flat ends of the separating wall.

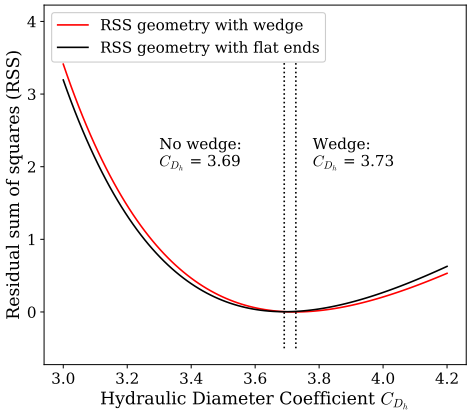

Figure 10: Calculations of the RSS values for simulations with and without a 10° wedge at the ends of the wall.

4.3. OSA Patient's Upper Airways Simulations

The aim of finding an improved version of the hydraulic diameter is to implement the improved version in the pragmatic model and achieve better results when simulating the flow the actual upper airways of an OSA patient. The results of implementing the averaged value of the two hydraulic diameter coefficients into the pragmatic model are shown in Fig. 11. In this figure the cutplanes correspond to the cutplanes from Fig. 3, which indicate the locations the results from the CFD simulations are taken from. The cross-sectional area and perimeter used as input for the pragmatic model have been extracted from the same 3D model at the numbered locations. The results with $C_{D_h} = 3.71$ in Eq. (7) only show a marginal improvement compared to using Eq. (6). The alternative hydraulic diameter coefficient, C_{D_h}, was applied to the first four cutplanes prior to the coinciding of the nasal passages indicated by the dashed and dotted line in Fig. 11, the standard hydraulic diameter $C_{D_h} = 4$ was used downstream of this. Further analyses showed that a more accurate coefficient for the human upper airways is given by $C_{D_h} = 1.80$. One of the reasons for this deviation is that the simple nature of the geometries analysed in this paper are better modeled by the a value closer to the original hydraulic diameter. The hydraulic diameter is meant for square ducts and other simple geometries, thus increasing the complexity of the geometry requires decreasing the hydraulic diameter.

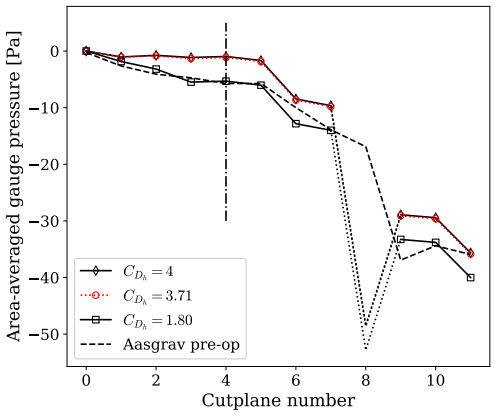

Figure 11: Pragmatic model simulations with cross-sections from Fig. 2 as input verified using CFD simulation performed through Aasgrav's specialization project (Aasgrav, 2017). The dashed and dotted line indicates where the nasal passages coincide.

5. Conclusions

As a part of creating a pragmatic flow simulator, the hydraulic diameter is used to transform the human upper airway geometry into a piping system. A test case has been created and presented in this paper to determine if this is a valid assumption to make in the nasal cavity. The test case used two variations of a simple duct-like geometry with a single duct to begin with, which goes over to a split up section with a separating wall between two passages and a coinciding geometry at the end of the wall. The simulations were performed assuming a laminar steady incompressible airflow that with a uniform velocity of 1 m/s at the inlet of the numerical domain. The results from these simulations showed the expected decline in the area-averaged gauge pressure over the length of the geometry. The resulting pressure curve was used as a basis for comparison to the pragmatic flow simulations. Pragmatic flow simulations were executed, with the only

loss contribution being the frictional losses. Comparing the results to the CFD simulations proved that the pressure slope generated by the pragmatic simulator was a little off. Analysing different values of the hydraulic diameter coefficient C_{D_h} for the two test cases presented gave two slightly different values. The two values were $C_{D_h} = 3.72$ and $C_{D_h} = 3.69$ for the case with and without a wedge at the leading and trailing ends of the wall respectively. Averaging the two values and implementing the new equation is given by $D_h = 3.71 \cdot \frac{A}{P_e}$ into the pragmatic model hardly improved its accuracy for flow in the upper airways of an OSA patient. However, $C_{D_h} = 1.80$ in the pragmatic model proved to give good agreement of the pressure with the CFD results. This investigation proved that the accuracy of the pragmatic simulations could be improved by altering the hydraulic diameter coefficient C_{D_h}. To conclude, the coefficients found in this study did not provide accurate results on the actual human upper airway, but imply that altering the hydraulic diameter can lead better accuracy. This implies that the redefinition of the hydraulic diameter proposed in this study can be used as an optimization parameter in the pragmatic model.

References

Aasgrav, E. (2017), CFD Simulations of Turbulent Flow in the Human Upper Airways, master's thesis, NTNU.

ANSYS (2021*a*), *Ansys® Fluent, 2021R2, User's Guide*.

ANSYS (2021*b*), *Ansys® Meshing, 2021R2, ANSYS Meshing User's Guide*.

ANSYS (2021*c*), *Ansys® Workbench, 2021R2, User's Guide*.

Cengel, Y. A. and Cimbala, J. M. (2010), *Fluid Mechanics: Fundamentals and Applications, 2^{nd} ed.*, McGraw Hill.

Fettman, N., Sanford, T. and Sindwani, R. (2009), 'Surgical management of the deviated septum: techniques in septoplasty', *Otolaryngologic Clinics of North America* **42**(2), 241–252.

Friedman, M., Vidyasagar, R., Bliznikas, D. and Joseph, N. (2005), 'Does severity of obstructive sleep apnea/hypopnea syndrome predict uvulopalatopharyngoplasty outcome?', *The Laryngoscope* **115**(12), 2109–2113.

Gharibeh, T. and Mehra, R. (2010), 'Obstructive sleep apnea syndrome: natural history, diagnosis, and emerging treatment options', *Nature and Science of Sleep* **2**, 233.

Jordal, M. R., Johnsen, S. G., Dahl, S. K. and Müller, B. (2017), 'Patient Specific Numerical Simulation of Flow in the Human Upper Airways for Assessing the Effect of Nasal Surgery', *Progress in Applied CFD - CFD - 2017* pp. 153–162.

Kezirian, E. J., Weaver, E. M., Yueh, B., Deyo, R. A., Khuri, S. F., Daley, J. and Henderson, W. (2004), 'Incidence of serious complications after uvulopalatopharyngoplasty', *The Laryngoscope* **114**(3), 450–453.

Kim, S. K., Na, Y., Kim, J.-I. and Chung, S.-K. (2013), 'Patient specific CFD models of nasal airflow: overview of methods and challenges', *Journal of Biomechanics* **46**(2), 299–306.

Lee, T. and Mateescu, D. (1998), 'Experimental and numerical investigation of 2D backward-facing step flow', *Journal of Fluids and Structures* **12**(6), 703–716.

Martonen, T. B., Quan, L., Zhang, Z. and Musante, C. (2002), 'Flow simulation in the human upper respiratory tract', *Cell Biochemistry and Biophysics* **37**(1), 27–36.

Matthias, C. (2007), 'Surgery of the nasal septum and turbinates', *GMS Current Topics in Otorhinolaryngology, Head and Neck Surgery* **6**.

Punjabi, N. M. (2008), 'The epidemiology of adult obstructive sleep apnea', *Proceedings of the American Thoracic Society* **5**(2), 136–143.

Sawyer, A. M., Gooneratne, N. S., Marcus, C. L., Ofer, D., Richards, K. C. and Weaver, T. E. (2011), 'A systematic review of CPAP adherence across age groups: clinical and empiric insights for developing CPAP adherence interventions', *Sleep Medicine Reviews* **15**(6), 343–356.

Sparrow, E., Abraham, J. and Minkowycz, W. (2009), 'Flow separation in a diverging conical duct: Effect of reynolds number and divergence angle', *International Journal of Heat and Mass Transfer* **52**(13-14), 3079–3083.

Weisz, T. G. (2021), Pragmatic modeling of flow in the human upper airways, Specialization project, NTNU.

Weisz, T. G. (2022), Pragmatic modeling of flow in the human upper airways for sleep apnea treatment, Master's thesis, NTNU.

White, F. M. (2008), *Fluid Mechanics, 6^{th} ed.*, McGraw Hill.

Wikipedia contributors (2022), 'Residual sum of squares — Wikipedia, the free encyclopedia'. [Online; accessed 29.05.2022].
URL: *https://en.wikipedia.org/wiki/Residual$_s$um$_o$f$_s$quares*